The cholesterol transfer protein GRAMD1A regulates autophagosome biogenesis

Laraia, Luca; Friese, Alexandra; Corkery, Dale P.; Konstantinidis, Georgios; Erwin, Nelli; Hofer, Walter; Karatas, Hacer; Klewer, Laura; Brockmeyer, Andreas; Metz, Malte

Total number of authors:
21

Published in:
Nature Chemical Biology

Link to article, DOI:
10.1038/s41589-019-0307-5

Publication date:
2019

Document Version
Peer reviewed version

The cholesterol transfer protein GRAMD1A regulates autophagosome biogenesis

Luca Laraia[1,2,#], Alexandra Friese[1,#], Dale P. Corkery[3,4], Georgios Konstantinidis[3,4], Nelli Erwin[5], Walter Hofer[1], Hacer Karatas[1], Laura Klewer[3], Andreas Brockmeyer[1], Malte Metz[1], Beate Schölermann[1], Mridula Dwivedi[5], Lei Li[5], Pablo Rios-Munoz[6,7], Maja Köhn[6,7], Roland Winter[5], Ingrid R. Vetter[1], Slava Ziegler[1], Petra Janning[1], Yao-Wen Wu[3,4,*], Herbert Waldmann[1,5,*]

[1]Max-Planck-Institute of Molecular Physiology, department of Chemical Biology, Otto-Hahn-Str. 11, 44227 Dortmund (Germany); [2]Technical University of Denmark, Department of Chemistry, Kemitorvet, Bygning 207, DK-2800 Kgs. Lyngby (Denmark); [3]Chemical Genomics Centre of the Max-Planck-Society, Otto-Hahn-Str. 15, 44227 Dortmund (Germany); [4]Department of Chemistry, Umeå University, 90187 Umeå, Sweden; [5]Faculty of Chemistry and Chemical Biology, Technical University Dortmund, Otto-Hahn-Str. 4a, 44227 Dortmund (Germany); [6]Centre for Biological Signalling Studies (BIOSS), University of Freiburg, Schänzlestrasse 18, 79104 Freiburg (Germany); [7]Faculty of Biology, University of Freiburg, Schänzlestrasse 18, 79104 Freiburg (Germany).

[#]Authors contributed equally to this work.

*Correspondence to: herbert.waldmann@mpi-dortmund.mpg.de; yaowen.wu@umu.se

Editorial Summary

The cholesterol transfer protein GRAMD1A was identified as the target of the autophagy inhibitors autogramin-1 and 2. GRAMD1A is required for autophagosome biogenesis, and autogramins represent tool compounds for studying this process.

Abstract

Autophagy mediates the degradation of damaged proteins, organelles and pathogens and plays a key role in health and disease. The identification of new mechanisms involved in autophagy regulation is of major interest. In particular little is known about the roles of lipids and lipid binding proteins in the early steps of autophagosome biogenesis. Through target agnostic, high-content, image-based identification of indicative phenotypic changes induced by small molecules, we have identified autogramins as a novel autophagy inhibitor class. Autogramins selectively target the recently discovered cholesterol transfer protein GRAM domain containing protein 1A (GRAMD1A), which had not been implicated in autophagy before, and directly compete with cholesterol binding to the GRAMD1A StART domain. GRAMD1A accumulates at sites of autophagosome initiation, affects cholesterol distribution in response to starvation and is required for autophagosome biogenesis. These findings identify a novel biological function of GRAMD1A and a new role for cholesterol in autophagy.

Introduction

Macroautophagy (hereafter autophagy) is a catabolic cellular process that is involved with clearing unwanted or damaged proteins and organelles, as well as pathogens, from cells[1]. During autophagy, double-membraned structures known as phagophores engulf cytoplasmic components and form autophagosomes, which subsequently fuse with lysosomes for cargo digestion[2]. Autophagy is fundamental to physiology and associated with human diseases, including both cancer suppression and promotion, as well as neurodegeneration[1-4]. Given the essentiality of this process, tools to understand autophagy at the molecular level are in continuing demand. High-content screening is valuable to rapidly identify autophagy modulators in a high-throughput manner, and has successfully been applied by our group and others to deliver new tool compounds to study autophagy[5-7].

Despite the fact that lipids are required to build up the autophagosome membrane, much is still unknown about their role, or the role of lipid-binding and transfer proteins, in autophagosome biogenesis[8]. Importantly, the proteins responsible for transferring lipids to the nascent autophagosomal membrane are unknown. However, their potential importance is underscored by the fact that certain lipids, e.g. phosphatidylinositol-3-phosphate (PI3P) are essential for autophagosome initiation and development[9-12]. Notably, the role of cholesterol, a major lipid constituent of the plasma membrane, in autophagy and autophagosome biogenesis has not been fully elucidated.

Here we report the identification of GRAMD1A as novel modulator of autophagy. A high content image-based phenotypic screen of a small-molecule library identified autogramins as autophagy inhibitors that selectively target the cholesterol-binding StART domain of GRAMD1A. We found that GRAMD1A, is a cholesterol transfer protein, required in early stages of autophagosome biogenesis. Our findings suggest that cholesterol plays an important role in autophagosome formation.

Results

Identification of autogramins as autophagy inhibitors

To identify small molecule autophagy inhibitors with new mechanisms of action, a high-content, image-based phenotypic screen was employed that quantifies autophagosomal structures in MCF7 cells after autophagy induction (Supplementary Table 1).[13-15] Briefly, autophagy was induced in MCF7 cells stably expressing EGFP-LC3 by amino acid starvation (starv.; Earle's balanced salt solution, EBSS) or by rapamycin (rapa.) treatment. Autophagosomal structures labeled by LC3 were quantified using automated microscopy and image analysis. From >150,000 compounds tested, those that inhibited autophagosome formation by >50% at 10 µM were re-screened. Confirmed hits were then tested in dose-response, and the most potent hits (IC_{50} < 1 µM) were taken forward for further study. Amongst those, the screen identified a class of aminothiazoles (**1-2**, Figure 1a) that reduced autophagosome

numbers by more than 70% at 10 µM, and displayed IC_{50}s in the nanomolar range[5,6,13]. Exploration of structure-activity relationships (SAR) (see supplementary discussion, Supplementary Table 2 as well as Supplementary Figure 1 and supplementary note "synthetic procedures" for synthesis) identified more potent inhibitors and a suitable attachment point for immobilization on solid phase for target identification experiments. Compounds **3** and **4** (Figure 1a), were termed autogramin-1 and 2, respectively, and chosen for further studies due to their favorable stability and solubility properties compared to **1**, which decomposed over time in organic solvent. Autogramin-2 in particular was used for biophysical experiments, which required higher compound concentrations due to its improved solubility even above 50 µM. Autogramins potently inhibited autophagy induced by either starvation (Figure 1b, d and Supplementary Figure 2) or mTORC1 inhibition (Figure 1c, d and Supplementary Figure 2), suggesting that they most likely target a protein downstream of mTORC1. Both compounds also inhibited LC3 lipidation and the degradation of p62 (Figure 1e and Supplementary Figure 2-4) and selectively inhibited growth of glucose-starved MCF7 cells over fed cells (Figure 1f and Supplementary Figure 2)[7,16].

Autogramins target GRAMD1A

For molecular target identification a probe (Figure 2a) that retained excellent potency was synthesized and employed in affinity-based proteomic experiments using MCF7 cell lysates obtained after autophagy induction by amino acid starvation. The only protein that was selectively enriched in a statistically significant manner was GRAM domain containing protein 1A (GRAMD1A) (for details see the Supplementary Information and Supplementary Figure 5). The members of the GRAMD1 protein family (GRAMD1A-C) contain a putative membrane signal, a GRAM domain, a StAR-related lipid transfer (StART) domain and a transmembrane helix (Supplementary Figure 6a)[17,18]. The GRAM domain is found in the context of a larger pleckstrin homology (PH) GRAM domain, which typically binds phosphoinositides[19,20]. Recently, the StART domains of GRAMD1A-C were reported to transfer cholesterol[21] and X-ray structures of the GRAM domain of the GRAMD1A yeast homologue lipid transfer at contact site (Ltc1/Lam6) and the StART domains of Lam2 and 4 were reported[21,22]. Very recently the role of GRAMD1A-C (renamed Aster A-C) in sterol transfer between the ER and the plasma membrane has been reported[23]. However, no structures of human GRAMD1A-C have been reported and their roles in mediating membrane contacts, particularly in the context of autophagy, are unclear. Furthermore, no tool compounds to interrogate this protein family have been reported.

Binding of GRAMD1A to the immobilized positive pull-down probe could be competed in a dose-dependent manner by autogramin-1 (Figure 2b). No binding to GRAMD1B was observed. Binding to GRAMD1C was weak and could also be competed. Target engagement for autogramin-2 in HeLa cells was confirmed using bioluminescence resonance energy transfer[24]. Bodipy-autogramin (Figure 2a) was

used as a tracer to detect binding to NanoLuc-tagged GRAMD1A StART domain. Autogramin-2 dose dependently displaced the tracer, whereas the inactive analog **8** donefailed to attenuate the BRET signal (Figures 2c and d). A cellular thermal shift assay (Figure 2e and f)[25] in MCF7 cell lysates and assessment of GRAMD1A stability by western blotting revealed an increase in melting temperature (T_m) of GRAMD1A by 2.1 °C, which confirmed the interaction of autogramin-1 and GRAMD1A in cell lysate. Thermal shift assays employing recombinant proteins containing StART (S) domains in differential scanning fluorimetry (DSF) experiments (Figure 2g) showed that autogramin-2 stabilizes GRAMD1A and to a lesser extent C but not B, further confirming the competitive pull-down results. In fluorescence polarization experiments, a Bodipy-labeled autogramin analogue bound to the StART domain of GRAMD1A with a K_d of 49 $\pm$ 12 nM (Figure 2h and Supplementary Figure 6j). This binding could be competed by unlabeled autogramin-2 (Supplementary Figure 6k). The GRAMD1A construct containing both PH-GRAM and StART domains showed a similar affinity to Bodipy-autogramin (K_d = 52 $\pm$ 4 nM), whereas the PH-GRAM construct alone did not bind, indicating that autogramins target the StART domain of GRAMD1A (Figure 2h and Supplementary Figure 6j). Comparison with the StART domains of GRAMD1B and C revealed a 200- and 580-fold higher K_d compared to GRAMD1A (Figure 2i and Supplementary Figure 6h-j), confirming that autogramins selectively bind to GRAMD1A as compared to B and C. Bodipy-autogramin also displayed almost three orders of magnitude selectivity over unrelated sterol binding proteins STARD1, STARD3, LXR-β and SCP-2 (Figure 2i), suggesting that excellent selectivity across entire families of sterol-binding proteins is possible. No significant binding of Bodipy-autogramin to other constructs of GRAMD1B and C could be detected (Supplementary Figure 6h-j).

Autogramins inhibit cholesterol binding and transfer by GRAMD1A

Quantitative assessment of cholesterol derivative binding to GRAMD1A-C by means of fluorescence polarization measurements employing 22-NBD-cholesterol as the tracer showed that the StART domains of GRAMD1A-C bound 22-NBD-cholesterol with high affinity (Figure 3a and Supplementary Figure 6b and d). Interestingly 6-NBD-cholesterol, in which the NBD dye is substituted at the 3-position of the A-ring, was not able to bind the GRAMD1A-C StART domains (Supplementary Figure 6c), suggesting that cholesterol binds to GRAMD1 proteins with its A-ring directed into the binding pocket. This data is consistent with the recently published report.[23] The PH-GRAM constructs of GRAMD1A-C bound 22-NBD-cholesterol with much lower affinity (Figure 3b, c and Supplementary Figure 6d), indicating that cholesterol binding occurs predominantly through the StART domain. Binding of 22-NBD-cholesterol to the GRAMD1A StART domain could be inhibited by autogramin-2 in a dose-dependent manner, but not by the inactive analogue **8** (Figure 3d and Supplementary Figure 6e), suggesting that the autogramin binding site of GRAMD1A overlaps with the cholesterol binding site. Autogramin-2 did not compete with 22-NBD-cholesterol binding to GRAMD1B and C, further confirming its selectivity for

GRAMD1A (Figure 3d and Supplementary Figure 6e). 25(OH)-cholesterol as a positive control was able to compete with binding of 22-NBD-cholesterol to all three GRAMD1 proteins, while no A- or B-ring hydroxylated oxysterols were able to (Figure 3d and Supplementary Figures 6e and f).

The StART domain of GRAMD1A transferred cholesterol from donor liposomes containing 23-Bodipy-cholesterol and rhodamine labeled 1,2-dihexadecanoyl-sn-glycero-3-phosphoethanolamine (DHPE) to acceptor liposomes without fluorescent lipids as indicated by a decrease in FRET signal, which could be inhibited by autogramin-2 (Figure 3e and Supplementary Figure 6g). The GRAMD1A StART domain alone transferred cholesterol more efficiently than the construct containing both the PH-GRAM and StART domains (Figure 3f). The PH-GRAM construct alone did not transfer cholesterol. The StART domains of GRAMD1B and C also transferred cholesterol, but this could not or only to a minor extent be inhibited by autogramin-2 (Figure 3e and Supplementary Figure 6g). The ability of GRAMD1A to transfer cholesterol was further strengthened by AFM experiments with DOPC/DPPC/cholesterol (1:2:1) lipid membranes. The GRAMD1A StART domain significantly disturbed the organization of coexisting liquid-ordered (l_o) and liquid-disordered (l_d) phase domains, causing an apparent decrease in l_o phase (Figure 3g). Interestingly, the GRAMD1A StART domain formed non-healing holes in the membrane in a time dependent manner, which might be a direct consequence of cholesterol extraction.

GRAMD1 proteins are predicted to bind phosphoinositides through their GRAM domains[17,18]. GRAMD1A, B and C constructs containing either only the PH-GRAM domain or both PH-GRAM and StART domains bound to different phosphatidyl inositol phosphates (PIPs), spotted on a hydrophobic membrane, with the same pattern and with strongest affinity to PI3P, PI4P and PI5P, and with lower affinity to $PI(3,4)P_2$, $PI(3,5)P_2$ and $PI(4,5)P_2$ (Supplementary Figure 7a). No binding could be detected for the StART domains. Binding of GRAMD1A could not be competed with autogramin-2 or 25(OH)-cholesterol, suggesting that autogramins target the StART domain of GRAMD1A leaving the function of the PH-GRAM domain unaffected (Supplementary Figure 7b).

Hydrogen deuterium exchange mass spectrometry (HDX-MS) experiments revealed that in the presence of both 25(OH)-cholesterol (Figure 4a) or autogramin-2 (Figure 4b) H-D exchange was reduced for amino acids 397-405, 426-440, 464-473 and 507-529 (see Supplementary Figure 8a for representative deuterium uptake plots) indicating a common binding site.

While we could not determine the structure of the GRAMD1A StART domain, the structure of the GRAMD1C StART domain was successfully determined (Supplementary Table 3). The protein crystallized in space group $P2_1$ with one molecule per asymmetric unit with a domain fold similar to

structures determined for other previously reported StART domains (Supplementary Figure 8b)[22]. It consists of a 7-stranded antiparallel β-sheet, two shorter N-terminal α-helices (α1 and α2) and one 34-aa long C-terminal α-helix (α3). The β-sheet, which folds into a half-barrel structure, wraps around helix α3, thereby forming a helix-grip fold. The β-sheet and helix α3 form a narrow hydrophobic tunnel that is bordered by helices α2 and α3 on one side, and β3-β4 (so-called Ω1) and β5-β6 (so-called Ω2) loops on the other side. This cavity of GRAMD1C is large enough to accommodate a single cholesterol molecule predominantly via hydrophobic interactions, as confirmed by docking experiments (Supplementary Figure 8c). In our crystal structure of the GRAMD1C StART domain the cavity is filled with five 2-methyl-2,4-pentanediol (MPD) molecules originating from the crystallization buffer, which indicates that the binding pocket is not completely hydrophobic, especially towards the bottom of the tunnel. Thus, a network of water-mediated hydrogen bonds, as described for Lam2[21], might also play a role in the interaction between the 3-hydroxyl group of cholesterol and the bottom of the cavity in GRAMD1C.

Structural comparison by a DALI search against the Protein Data Bank[26] revealed the StART domains of Lam2 (PDB-ID: 6CAY, 5YS0, 5YQI and 5YQQ) and Lam4 (PDB-ID: 5YQJ, 6YBM and 6BYD), yeast homologues of the human GRAMD1 proteins, as most closely related structures, followed by various cyclases (e.g. the Zhui aromatase/cyclase, PDB-ID: 3TFZ) and pollen allergens, all belonging to the Bet v1-like superfamily according to the SCOP classification. This first structure of a mammalian StART domain and the Lam2/4 StART domains show the largest structural similarity near the ligand-binding site and the position of 25(OH)-cholesterol docked into the GRAMD1C structure is very similar to those of the sterols in the published Lam2/4 structures (Supplementary Figure 8d), indicating a sterol binding mechanism that is conserved from yeast to human. In contrast to the structures of ligand-bound Lam StART domains (PDB-ID: 6CAY and 5YS0), the Ω1 loop is open in our GRAMD1C apo structure, similar to the apo states of the Lam StART domains (PDB-ID: 6BYD and 5YQJ).

Analysis of a homology model of the GRAMD1A StART domain based on the crystal structure of the GRAMD1C StART domain (sequence identity ~45%) taking the results of the HDX-MS and docking experiments into account (Figure 4c-f), showed that 25(OH)-cholesterol and autogramin-2 share a similar binding region - located at the Ω1 and Ω2 loops, the loop following helix α2, and helix α3 near the tunnel entrance - and a similar hydrophobic binding mode with autogramin-2 extending further towards the entrance of the cavity as compared to cholesterol. Ligand binding was further characterized by means of mutational analysis of the binding site and quantitative binding analysis (Supplementary Figure 9). Residues of the GRAMD1A StART domain, which lie within the identified binding regions, were mutated to corresponding residues in GRAMD1B or C. Comparison of mutant and wild-type

GRAMD1A regarding their binding affinities to 22-NBD-cholesterol revealed that the mutations P428V (located at Ω1 loop), L510F (located at helix α3), S515F (located at helix α3) and G518S (located at helix α3) increased the dissociation constant by more than 2-fold, with the most drastic effects seen for S515F and G518S. Indeed, mutation at position G518 to a larger side chain has been described to affect sterol binding of yeast homologues Lam2 and Lam4[27], suggesting that the binding mode to Lam/GRAMD1 proteins is conserved from yeast to human. Comparing the binding affinities of mutant and wild-type GRAMD1A to Bodipy-autogramin, the G518S mutation increased the affinity by 2.3-fold, whereas the S515F mutation reduced it by 2.9-fold. Interestingly, the G466D (located at Ω2 loop) and G434T/P435G/A438T (short GPxxA, located at Ω1 loop) mutations reduced the binding affinity to Bodipy-autogramin by 2.4- and 3.4-fold, respectively, but affected 22-NBD-cholesterol binding only to a very minor extent, suggesting that autogramins bind closer to Ω1 and Ω2 loops as compared to cholesterol. Additionally, the presence of a flexible glycine residue in GRAMD1A (G434, compared to an alanine in GRAMD1B or threonine in GRAMD1C) and a proline residue (P428, compared to threonine in GRAMD1B and valine in GRAMD1C) might influence the conformation of the Ω1 loop such that the binding of autogramin-2 is strongly favored in GRAMD1A. Therefore, the residues of the Ω1 and Ω2 loops could be involved in determining the selectivity of autogramins for GRAMD1A over B and C.

GRAMD1A is required for autophagosome initiation

Involvement of GRAMD1A in autophagy regulation, and the stage of autophagy impacted by autogramins, was evaluated using MCF7 cells stably expressing mCherry-EGFP-LC3[28]. This reporter takes advantage of the differential pH sensitivity of mCherry and EGFP to discriminate between autophagic vesicles pre- and post-lysosomal fusion. Similar to treatment with the PI3 kinase inhibitor wortmannin, which inhibits autophagosome initiation[29], autogramin-1 induced a dose-dependent decrease in the number of autophagosomes following starvation (Figure 5a and b). In contrast, chloroquine, an inhibitor of autophagosome-lysosome fusion, induced accumulation of autophagosomes and decreased numbers of autolysosomes (Figure 5b). To differentiate between inhibition of autophagosome initiation and increased autophagic flux, phagophore formation was assessed in MCF7 cells stably expressing the phagophore marker EGFP-ATG5. Autogramin-1 treatment resulted in a dose-dependent decrease in phagophore formation in response to starvation (Figure 5c) and reduction of LC3-II accumulation after chloroquine treatment (Figure 5d). Thus, inhibition of GRAMD1A function by autogramin-1 impairs autophagosome initiation, suggesting a role for GRAMD1A in autophagosome biogenesis. To dissect the function of GRAMD1A in autophagosome biogenesis, WIPI2 dynamics were analyzed by imaging EGFP-WIPI2b stable cell lines under starvation in the presence or absence of autogramin-1 (Figure 5e). Autogramin-1 did not significantly reduce the total number of EGFP-WIPI2b foci, suggesting that GRAMD1A acts downstream of PI3P synthesis in

the autophagosome formation pathway. Interestingly, autogramin-1 treatment increased the duration of EGFP-WIPI2b foci suggesting stalled phagophore formation. Silencing of GRAMD1A expression in MCF7 cells using two independent siRNAs resulted in a modest decrease in LC3-II accumulation (Figure 5f) and significant inhibition of LC3 puncta formation (Figure 5g) in chloroquine treated cells. Given the documented redundancy amongst lipid transfer proteins[30], and the time available for cellular adaptation when using traditional genetic approaches like RNA interference, these muted responses support the role of GRAMD1A in regulating autophagosome biogenesis. To assess whether cells were in fact adapting to GRAMD1A knockdown, we monitored the effect on autophagy over a period of 72 hours (Supplementary Figure 11). Whilst after 24 hours GRAMD1A knockdown led to a robust inhibition of LC3 puncta formation, this effect was almost completely reversed after 72 hours, despite high levels of knockdown in both cases. This suggests that other, as yet undetermined, cholesterol transfer proteins are able to carry out GRAMD1A's function in autophagy. These results also stress the importance of chemical perturbation for evaluating novel functions of lipid transfer proteins.

GRAMD1A localization at sites of autophagosome biogenesis was confirmed by co-transfection of MCF7 cells with GRAMD1A and WD repeat domain phosphoinositide-interacting protein 1 (WIPI1), a marker of early autophagic structures, which binds to PI3P (Supplementary Figure 12). After starvation GRAMD1A was found to accumulate at WIPI1-positive foci. Live-cell microscopy of HeLa cells co-transfected with mCherry-tagged GRAMD1A and EGFP-tagged WIPI1 or LC3 showed that after starvation GRAMD1A enrichment occurred simultaneously with the recruitment of WIPI1 (Figure 6a, c and Movie S1). This GRAMD1A-enriched region of the ER persists after the loss of WIPI1 and becomes the site of LC3 foci formation (Figure 6b, c and Movie S2). LC3-positive autophagsomes increase in size and remain associated with GRAMD1A enriched regions of the ER before trafficking towards the perinuclear region of the cell (Movie S3); an event that has been shown to be regulated by the cholesterol sensor ORP1L[31].

Modulation of cellular cholesterol distribution by GRAMD1A inhibition was investigated through staining with filipin to visualize free cholesterol. Starvation in the presence of chloroquine resulted in an increase in intracellular cholesterol level (Figure 6d), partially attributed to the accumulation of cholesterol-enriched lysosomes and mature autophagosomes prior to fusion with lysosomes (Supplementary Figure 13). Treatment with autogramin-1 blocked cholesterol accumulation (Figure 6d), providing further support for the role of GRAMD1A-mediated cholesterol transfer in autophagosome initiation.

Discussion

Through discovery and application of autogramins as the first selective inhibitors of the cholesterol transfer protein GRAMD1A, we have demonstrated that GRAMD1A is involved in the regulation of autophagy, and appears to be required for biogenesis of the autophagosome. Cholesterol has an important role in regulating autophagosome transport[31] and maturation[32], but a role in autophagosome biogenesis has not been described before. GRAMD1A is recruited to the site of autophagosome initiation and inhibition of its cholesterol transfer activity by autogramins is sufficient to inhibit autophagosome biogenesis. Our findings imply that cholesterol transfer by GRAMD1A is required for autophagosome biogenesis.

The StART-like protein family is involved in transport of cholesterol[27,33,34] in humans and in budding yeast. The yeast protein Ltc1/Lam6 localizes at several membrane contact sites, including the ER-mitochondrial encounter structure (ERMES), ER-vacuole contact sites, vacuole and mitochondria patch (vCLAMP), and nuclear vacuolar junction (NVJ), and is probably important for interorganellar communication. The formation of sterol-enriched vacuolar membrane domains by Ltc1 plays a role in the regulation of TORC1/C2 signaling[35]. GRAMD1A is the mammalian homolog of Ltc1. It specifically binds to PI3P, PI4P and PI5P via its PH-GRAM domain (current study), and its PH-GRAM domain is required for GRAMD1A localization at the ER-PM membrane contact sites[36]. Upon autophagy induction GRAMD1A accumulates at the autophagosome initiation sites in the ER, potentially due to the enrichment of PI3P in these sites. GRAMD1A appears to be directly engaged in initiation of autophagosome biogenesis through regulation of cholesterol homeostasis at phagophores/autophagosomes. The cholesterol content of autophagosomal membranes increases as the autophagosome matures[37], due in part to fusion events with cholesterol rich lysosomes and late endosomes. Elevated membrane cholesterol has been recently shown to regulate late autophagosome transport in an event mediated by the cholesterol-sensing protein ORP1L[31]. Our data suggest that cholesterol plays an additional role in regulating early events in autophagosome initiation/phagophore expansion. The physiological consequence of GRAMD1A's cholesterol transfer ability had previously been unclear, and it still remains to be shown conclusively whether GRAMD1A can transfer cholesterol in cells. Taken together, the discovery of autogramins as GRAMD1A inhibitors connected the functional role of GRAMD1A to autophagy, and provided new insights into the physiological consequence of GRAMD1A's cholesterol transfer ability, showing that GRAMD1A activity appears to be required for autophagosome biogenesis. The chemical tools we describe will be instrumental in further defining its function within autophagy and related, cholesterol-mediated processes.

Acknowledgments

This work was supported by Max Planck Society to H.W., and by DFG grant (no.: SPP 1623), ERC (ChemBioAP), Vetenskapsrådet (Nr. 2018-04585), and The Knut and Alice Wallenberg Foundation to Y-W.W. Lu.La. was supported by a fellowship from the Alexander von Humboldt Stiftung. D.P.C. is supported by a fellowship from the Canadian Institute of Health Research (MFE-152550). We thank Dr. Sonja Sievers and the Compound Management and Screening Center (COMAS), Dortmund, Germany, for compound screening. We thank Raphael Gasper-Schönenbrücher, Kathrin Estel and the beamline staff for help with data collection at the SLS, Villigen, Switzerland. We thank Sharon Tooze for the kind gift of EGFP-WIPI2b cells. We acknowledge the Biochemical Imaging Center (BICU) at Umeå University and the National Microscopy Infrastructure, NMI (VR-RFI 2016-00968) for providing assistance in microscopy.

Author contributions

Lu.La. carried out the analogue and probe synthesis, the SAR analysis, the initial biological compound validation and the proteomic target identification and initial target validation. A.F. carried out the cloning, expression and purification of all recombinant proteins as well as all FP, DSF, PIP-binding, and crystallography experiments. A.F., A.B. and M.M. performed HDX-MS experiments. D.P.C. carried out cell biological characterization of GRAMD1A. G.K. and L.K. carried out autogramin validation experiments. W.H. and H.K. carried out the synthesis of the fluorescent probe. B.S. performed nanoBRET experiments. N.E. and Le.Li. carried out the cholesterol transfer experiments. M.D. performed AFM experiments. R.W. supervised cholesterol transfer and AFM experiments. P.J. carried out the MS-proteomics analysis. I.V. analyzed crystallographic data and performed homology modeling and docking experiments. P.R. and M.K. provided reagents. All authors analyzed data. Lu.La., A.F., D.P.C., G.K.. Y-W. W. and H.W. wrote the paper with comments from all other co-authors.

References

1. Mizushima, N., Levine, B., Cuervo, A.M. & Klionsky, D.J. Autophagy fights disease through cellular self-digestion. *Nature* **451**, 1069 (2008).

2. Mizushima, N., Yoshimori, T. & Ohsumi, Y. The Role of Atg Proteins in Autophagosome Formation. *Ann. Rev. Cell. Dev. Biol.* **27**, 107-132 (2011).

3. Rubinsztein, D.C., Codogno, P. & Levine, B. Autophagy modulation as a potential therapeutic target for diverse diseases. *Nat. Rev. Drug Discov.* **11**, 709-730 (2012).

4. White, E. Deconvoluting the context-dependent role for autophagy in cancer. *Nat. Rev. Cancer* **12**, 401-410 (2012).

5. Laraia, L. et al. Discovery of Novel Cinchona-Alkaloid-Inspired Oxazatwistane Autophagy Inhibitors. *Angew. Chem. Int. Ed.* **56**, 2145-2150 (2017).

6. Robke, L. et al. Phenotypic Identification of a Novel Autophagy Inhibitor Chemotype Targeting Lipid Kinase VPS34. *Angew. Chem. Int. Ed.* **56**, 8153-8157 (2017).

7. Robke, L. et al. Discovery of the novel autophagy inhibitor aumitin that targets mitochondrial complex I. *Chem. Sci.* **9**, 3014-3022 (2018).

8. Dall'Armi, C., Devereaux, Kelly A. & Di Paolo, G. The Role of Lipids in the Control of Autophagy. *Curr. Biol.* **23**, R33-R45 (2013).

9. Nascimbeni Anna, C., Codogno, P. & Morel, E. Phosphatidylinositol-3-phosphate in the regulation of autophagy membrane dynamics. *FEBS J.* **284**, 1267-1278 (2017).

10. Petiot, A., Ogier-Denis, E., Blommaart, E.F.C., Meijer, A.J. & Codogno, P. Distinct Classes of Phosphatidylinositol 3′-Kinases Are Involved in Signaling Pathways That Control Macroautophagy in HT-29 Cells. *J. Biol. Chem.* **275**, 992-998 (2000).

11. Kihara, A., Noda, T., Ishihara, N. & Ohsumi, Y. Two Distinct Vps34 Phosphatidylinositol 3–Kinase Complexes Function in Autophagy and Carboxypeptidase Y Sorting in Saccharomyces cerevisiae. *J. Cell Biol.* **152**, 519 (2001).

12. Dooley, Hannah C. et al. WIPI2 Links LC3 Conjugation with PI3P, Autophagosome Formation, and Pathogen Clearance by Recruiting Atg12–5-16L1. *Mol. Cell* **55**, 238-252 (2014).

13. Konstantinidis, G., Sievers, S. & Wu, Y.-W. Identification of Novel Autophagy Inhibitors via Cell-Based High-Content Screening. in *Methods Mol. Biol.* 1-9 (Humana Press, Totowa, NJ, 2018).

14. Balgi, A.D. et al. Screen for Chemical Modulators of Autophagy Reveals Novel Therapeutic Inhibitors of mTORC1 Signaling. *PLoS ONE* **4**, e7124 (2009).

15. Peppard, J.V. et al. Identifying Small Molecules which Inhibit Autophagy: a Phenotypic Screen Using Image-Based High-Content Cell Analysis. *Curr. Chem. Genom. Trans. Med.* **8**, 3-15 (2014).

16. Liu, J. et al. Beclin1 Controls the Levels of p53 by Regulating the Deubiquitination Activity of USP10 and USP13. *Cell* **147**, 223-234 (2011).

17. Wong, Louise H. & Levine, Tim P. Lipid transfer proteins do their thing anchored at membrane contact sites… but what is their thing? *Biochem. Soc. Trans.* **44**, 517 (2016).

18. Khafif, M., Cottret, L., Balagué, C. & Raffaele, S. Identification and phylogenetic analyses of VASt, an uncharacterized protein domain associated with lipid-binding domains in Eukaryotes. *BMC Bioinformatics* **15**, 222 (2014).

19. Doerks, T., Strauss, M., Brendel, M. & Bork, P. GRAM, a novel domain in glucosyltransferases, myotubularins and other putative membrane-associated proteins. *Trends Biochem. Sci.* **25**, 483-485 (2000).

20. Begley, M.J. et al. Crystal Structure of a Phosphoinositide Phosphatase, MTMR2: Insights into Myotubular Myopathy and Charcot-Marie-Tooth Syndrome. *Mol. Cell* **12**, 1391-1402 (2003).

21. Horenkamp, F.A., Valverde, D.P., Nunnari, J. & Reinisch, K.M. Molecular basis for sterol transport by StART-like lipid transfer domains. *EMBO J.* **37**, e98002 (2018).

22. Tong, J., Manik, M.K. & Im, Y.J. Structural basis of sterol recognition and nonvesicular transport by lipid transfer proteins anchored at membrane contact sites. *Proc. Nat. Ac. Sci. USA* **115**, E856 (2018).

23. Sandhu, J. et al. Aster Proteins Facilitate Nonvesicular Plasma Membrane to ER Cholesterol Transport in Mammalian Cells. *Cell* **175**, 514-529.e20 (2018).

24. Robers, M.B. et al. Target engagement and drug residence time can be observed in living cells with BRET. *Nat. Commun.* **6**, 10091 (2015).

25. Jafari, R. et al. The cellular thermal shift assay for evaluating drug target interactions in cells. *Nat. Protocols* **9**, 2100-2122 (2014).

26. Holm, L. & Rosenström, P. Dali server: conservation mapping in 3D. *Nuc. Acids Res.* **38**, W545-W549 (2010).

27. Gatta, A.T. et al. A new family of StART domain proteins at membrane contact sites has a role in ER-PM sterol transport. *eLife* **4**, e07253 (2015).

28. Kimura, S., Noda, T. & Yoshimori, T. Dissection of the Autophagosome Maturation Process by a Novel Reporter Protein, Tandem Fluorescent-Tagged LC3. *Autophagy* **3**, 452-460 (2007).

29. Blommaart Edward, F.C., Krause, U., Schellens Jacques, P.M., Vreeling-Sindelárová, H. & Meijer Alfred, J. The Phosphatidylinositol 3-Kinase Inhibitors Wortmannin and LY294002 Inhibit Autophagy in Isolated Rat Hepatocytes. *Eur. J. Biochem.* **243**, 240-246 (2004).

30. Ikonen, E. Cellular cholesterol trafficking and compartmentalization. *Nat. Rev. Mol. Cell Biol.* **9**, 125 (2008).

31. Wijdeven, R.H. et al. Cholesterol and ORP1L-mediated ER contact sites control autophagosome transport and fusion with the endocytic pathway. *Nat. Commun.* **7**, 11808 (2016).

32. Sarkar, S. et al. Impaired Autophagy in the Lipid-Storage Disorder Niemann-Pick Type C1 Disease. *Cell Rep.* **5**, 1302-1315 (2013).

33. Murley, A. et al. Ltc1 is an ER-localized sterol transporter and a component of ER–mitochondria and ER–vacuole contacts. *J. Cell Biol.* **209**, 539 (2015).

34. Elbaz-Alon, Y. et al. Lam6 Regulates the Extent of Contacts between Organelles. *Cell Rep.* **12**, 7-14 (2015).

35. Murley, A. et al. Sterol transporters at membrane contact sites regulate TORC1 and TORC2 signaling. *J. Cell Biol.* **216**, 2679-2689 (2017).

36. Besprozvannaya, M. et al. GRAM domain proteins specialize functionally distinct ER-PM contact sites in human cells. *eLife* **7**, e31019 (2018).

37. Punnonen, E.-L., Pihakaski, K., Mattila, K., Lounatmaa, K. & Hirsimäki, P. Intramembrane particles and filipin labelling on the membranes of autophagic vacuoles and lysosomes in mouse liver. *Cell. Tissue Res.* **258**, 269-276 (1989).

38. Cox, J. & Mann, M. MaxQuant enables high peptide identification rates, individualized p.p.b.-range mass accuracies and proteome-wide protein quantification. *Nat. Biotech.* **26**, 1367 (2008).

39. Tyanova, S. & Cox, J. Perseus: A Bioinformatics Platform for Integrative Analysis of Proteomics Data in Cancer Research. in *Cancer Systems Biology: Methods and Protocols* (ed. von Stechow, L.) 133-148 (Springer New York, New York, NY, 2018).

40. Hashimoto, Y., Zhang, S. & Blissard, G.W. Ao38, a new cell line from eggs of the black witch moth, Ascalapha odorata (Lepidoptera: Noctuidae), is permissive for AcMNPV infection and produces high levels of recombinant proteins. *BMC Biotech.* **10**, 50 (2010).

41. Oishi, H., Takaoka, Y., Nishimaki-Mogami, T., Saito, H. & Ueda, M. A Novel Nuclear Receptor Ligand, Digoxigenin, is a Selective Antagonist of Liver-X-receptors. *Chem. Lett.* **46**, 313-314 (2016).

42. Kernstock, R.M. & Girotti, A.W. Lipid transfer protein binding of unmodified natural lipids as assessed by surface plasmon resonance methodology. *Anal. Biochem.* **365**, 111-121 (2007).

43. Fang, J., Rand, K.D., Beuning, P.J. & Engen, J.R. False EX1 signatures caused by sample carryover during HX MS analyses. *Int. J. Mass Spec.* **302**, 19-25 (2011).

44. Kabsch, W. XDS. *Acta Crystallogr. D Biol. Crystallogr.* **66**, 125-132 (2010).

45. Adams, P.D. et al. PHENIX: a comprehensive Python-based system for macromolecular structure solution. *Acta Crystallogr. D Biol. Crystallogr.* **66**, 213-221 (2010).

46. Emsley, P., Lohkamp, B., Scott, W.G. & Cowtan, K. Features and development of Coot. *Acta Crystallogr. D Biol. Crystallogr.* **66**, 486-501 (2010).

47. Šali, A. & Blundell, T.L. Comparative Protein Modelling by Satisfaction of Spatial Restraints. *J. Mol. Biol.* **234**, 779-815 (1993).

48. Jones, G., Willett, P., Glen, R.C., Leach, A.R. & Taylor, R. Development and validation of a genetic algorithm for flexible docking. *J. Mol. Biol.* **267**, 727-748 (1997).

49. Laskowski, R.A. & Swindells, M.B. LigPlot+: Multiple Ligand–Protein Interaction Diagrams for Drug Discovery. *J. Chem. Inf. Mod.* **51**, 2778-2786 (2011).

50. Itakura, E. & Mizushima, N. Characterization of autophagosome formation site by a hierarchical analysis of mammalian Atg proteins. *Autophagy* **6**, 764-776 (2010).

51. de Chaumont, F. et al. Icy: an open bioimage informatics platform for extended reproducible research. *Nat. Methods* **9**, 690 (2012).

Figures

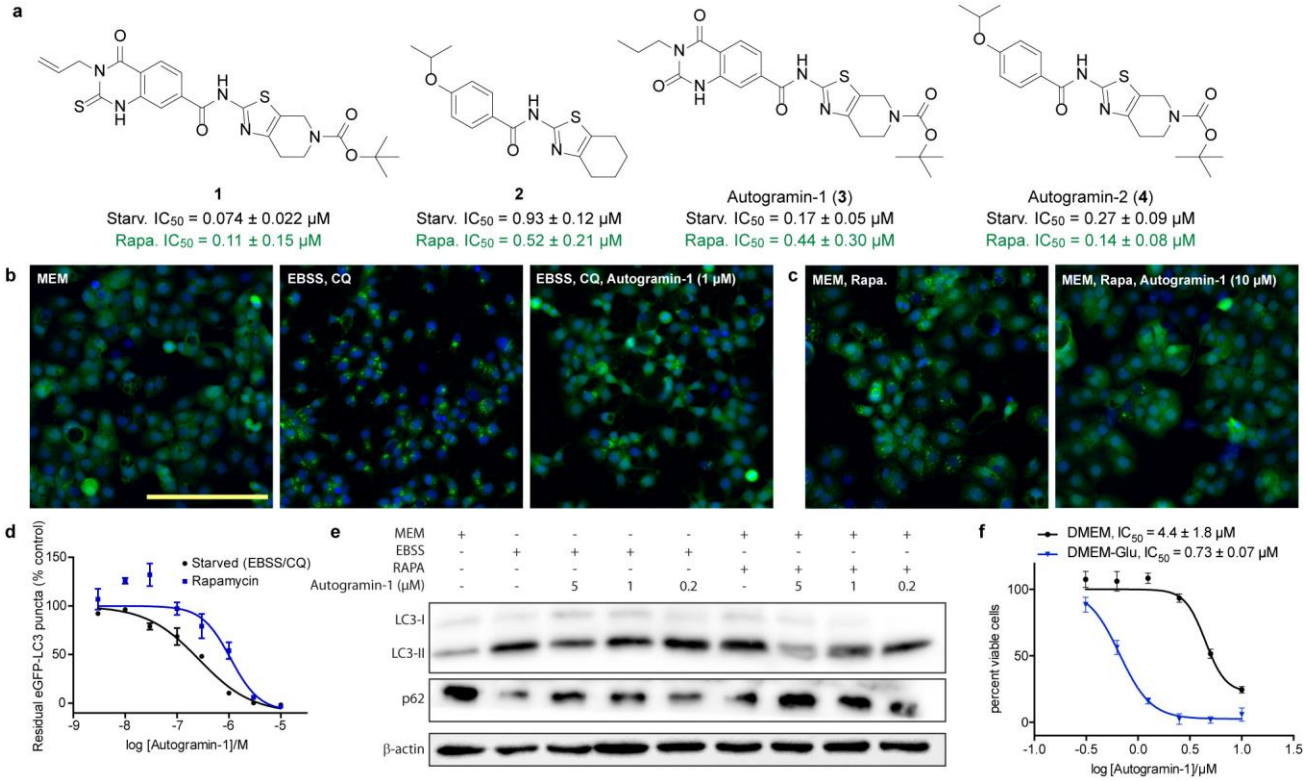

Figure 1. Autogramins inhibit autophagy. (a) Autophagy inhibitors identified through phenotypic screening; data is mean ± SEM (n = 3). (b) Effect of autogramin-1 (1 μM) on the accumulation of autophagosomes (visualized as green puncta) upon autophagy induction by amino acid starvation in MC7 cells stably transfected with eGFP-LC3. Scale bar = 110 μm. (c) Effect of autogramin-1 (10 μM) on accumulation of autophagosomes upon rapamycin (100 nM) treatment. (d) Quantification of autophagy activity for images in (b) and (c). Residual activity refers to the % of puncta remaining after compound treatment when compared to the negative control (EBSS/CQ). n = 3 with consistent results, representative images and data shown. (e) Effect of autogramin-1 on the lipidation of LC3 to LC3-II and p62 degradation in MCF7-LC3 cells following autophagy induction using amino acid starvation (EBSS) or rapamycin (RAPA, 100 nM) treatment. n = 3, representative blot shown (uncropped blots shown in Supplementary Figure 3). (f) Growth inhibitory effect of autogramin-1 on glucose-starved (0 mM glucose) or fed (25 mM glucose) MCF7 cells, as assessed by WST-1 assay. Data shown for t = 48 h. All data is mean ± SEM and is representative of three independent biological replicates carried out in triplicate.

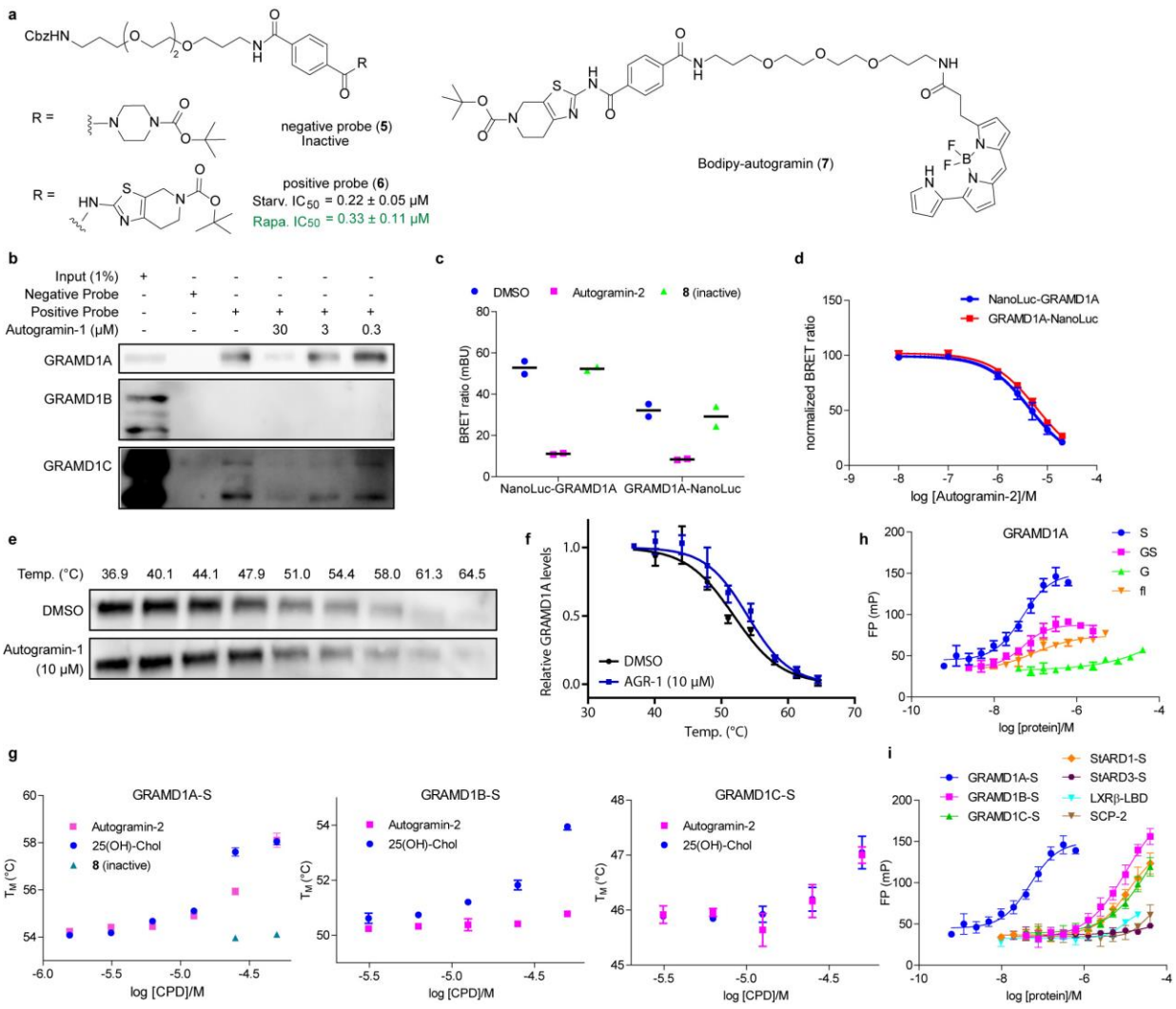

Figure 2. Autogramins target GRAMD1A. (a) Structures of pull-down probes and fluorescent tracer Bodipy-autogramin; data is mean ± SEM (n = 3). (b) Competitive pull-down using probes synthesized in (a). n = 3, representative blots shown (uncropped blots shown in Supplementary Figure 3). (c) NanoBRET assays with N- or C-terminal NanoLuc fusion to GRAMD1A StART domain using 0.5 µM Bodipy-Autogramin as tracer and 20 µM Autogramin-2 or compound **8** (negative control) as competitor. Data is mean of two independent experiments carried out in triplicate (n = 2, N = 3). (d) NanoBRET assays with N- or C-terminal NanoLuc fusion to GRAMD1A StART domain using 0.5 µM Bodipy-Autogramin as tracer and increasing concentrations of autogramin-2 as competitor. Data shown as mean ± SD of a representative experiment (n = 2, N = 3). IC_{50} value of competition is 4.7 µM for NanoLuc-GRAMD1A and 6.4 µM for GRAMD1A-NanoLuc. (e) Cellular thermal shift assay. Autogramin-1 stabilizes GRAMD1A towards melting. n = 3, representative blot shown (uncropped blots shown in Supplementary Figure 3). (f) Quantification of band intensity (mean ± s.e.m.) for three independent experiments shown in (e). T_m (DMSO) = 51.7 ± 0.1 °C, T_m (Autogramin-1) = 53.7 ± 1.0 °C. (g) Melting temperatures for GRAMD1A-C StART (S) domains in presence of different concentrations of 25(OH)-

cholesterol or autogramin-2, respectively, as assessed by differential scanning fluorimetry (DSF). Data shown as mean ± SD (n = 3). (h) Fluorescence polarization assay with Bodipy-autogramin and increasing concentrations of GRAMD1A constructs containing StART domain (S), PH-GRAM domain (G, ranges from the N-terminus to the beginning of the StART domain) or both domains (GS, ranges from the N-terminus to the beginning of the transmembrane helix); data shown as mean ± SD (n = 4). (i) Fluorescence polarization assay with Bodipy-autogramin and increasing concentrations of GRAMD1A-C StART domain (S) as well as the sterol binding domains of proteins from other known sterol-binding and transferring protein families. Data shown as mean ± SD (n = 4). K_d values for panels (g) and (h) are reported in Supplementary Figure 6d.

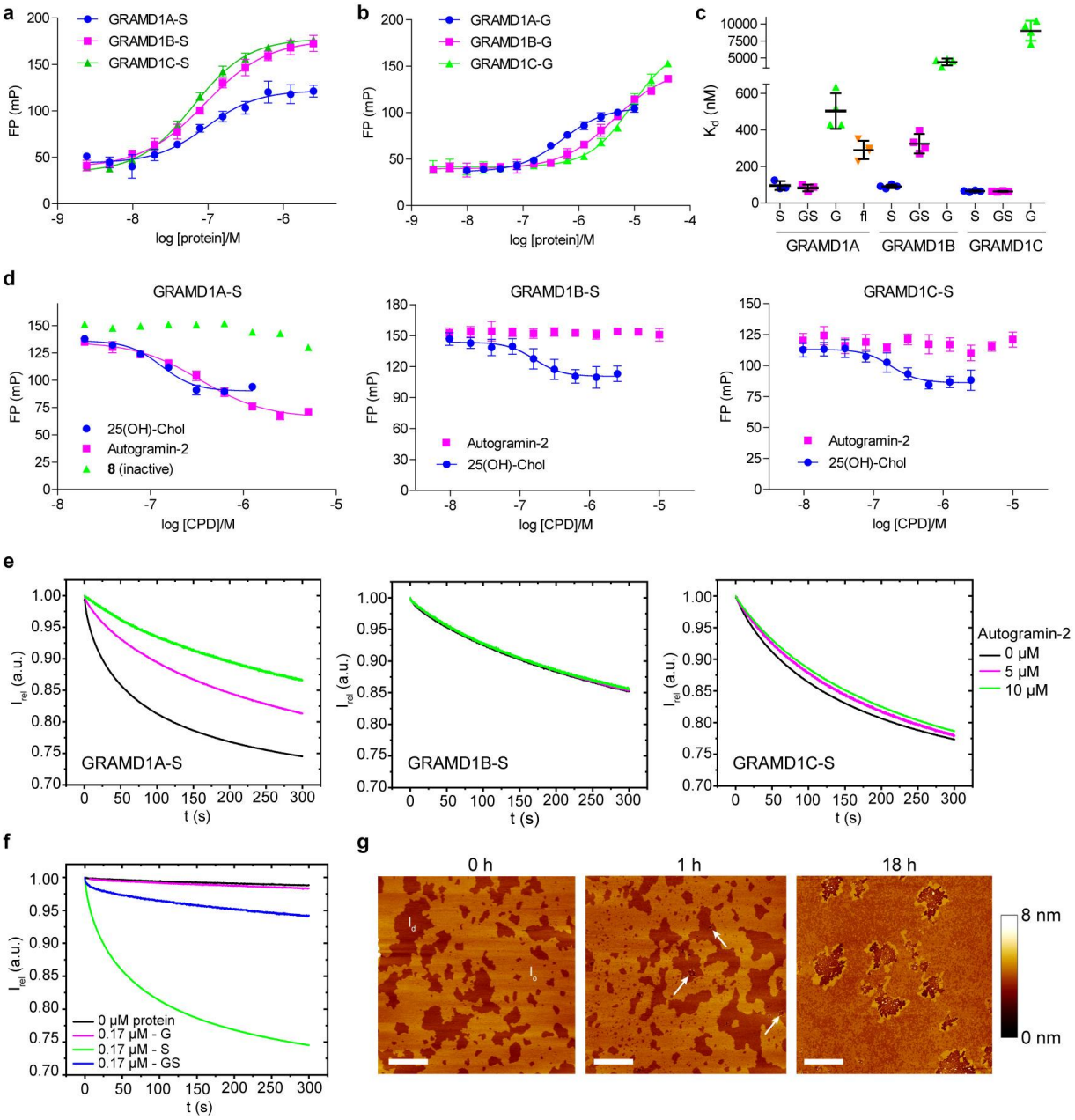

Figure 3. The cholesterol binding and transport activity of the GRAMD1A StART domain is inhibited by autogramins. (a) Fluorescence polarization assay with 22-NBD-cholesterol and increasing concentrations of the StART domains (S) of GRAMD1A-C. (b) Fluorescence polarization assay with 22-NBD-cholesterol and increasing concentrations of the PH-GRAM constructs (G) of GRAMD1A-C (range from the N-terminus to the beginning of the StART domain). (c) Dissociation constants for 22-NBD-cholesterol binding to GRAMD1A-C constructs calculated from fluorescence polarization assays shown in (a), (b) and Supplementary Figure 6b. (d) Fluorescence polarization

assays with 22-NBD-cholesterol, StART domains (S) of GRAMD1A-C and increasing concentrations of 25(OH)-cholesterol, autogramin-2 or **8** (negative control), respectively. All data in (a-d) shown as mean ± SD (n = 4). IC_{50} values of competition assays with 25(OH)-cholesterol are 137 ± 27 nM (K_i = 114 nM), 168 ± 42 nM (K_i = 137 nM) and 189 ± 71 nM (K_i = 145 nM) for GRAMD1A, B and C, respectively. IC_{50} value of competition assay with GRAMD1A-S and autogramin-2 is 349 ± 51 nM (K_i = 290 nM). (e) Cholesterol transfer assays with the StART domains (S) of GRAMD1A-C in absence and presence of autogramin-2. n = 3, representative data shown. (f) Cholesterol transfer assays with the PH-GRAM construct (G), StART domain (S) and a construct containing both PH-GRAM and StART domain (GS) of GRAMD1A. n = 3, representative data shown. (g) Representative AFM images of a DOPC/DPPC/cholesterol (1:2:1) lipid membrane with coexisting domains in l_o and l_d phase before (0 h) and after (1 h and 18 h) addition of GRAMD1A StART domain (n = 3). Scale bars: 2 µm.

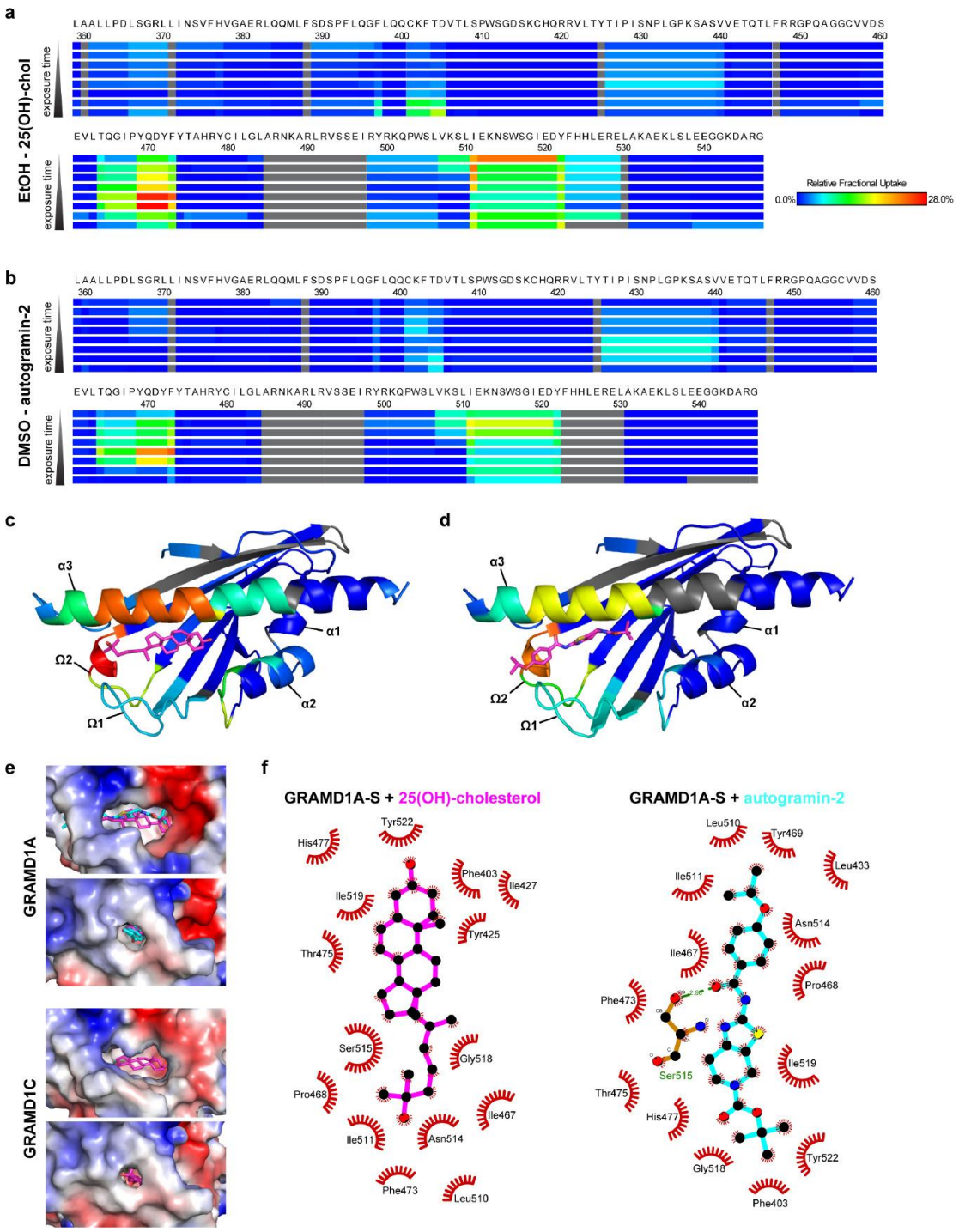

Figure 4. Cholesterol and autogramins target the same binding site within the GRAMD1A StART domain. (a) Heat maps showing the relative fractional deuterium uptake of the GRAMD1A StART domain (S) in presence of 25-(OH)-cholesterol compared to GRAMD1A-S in presence of equivalent amounts of ethanol only, as assessed by HDS-MS experiments. Experiments were performed at following exposure times (from top to bottom): 15 s, 30 s, 45 s, 1 min, 3 min, 10 min, 30 min and 1 h.

Coloring according to spectrum bar. Grey coloring means no assignment of respective residue/peptide during MS analysis. (b) Heat maps showing the relative fractional deuterium uptake of the GRAMD1A StART domain (S) in presence of autogramin-2 compared to GRAMD1A-S in presence of equivalent amounts of DMSO only, as assessed by HDS-MS experiments. Coloring as in (a). (c-d) Homology model of GRAMD1A StART domain with docked cholesterol (c) or autogramin-2 (d), respectively. Coloring of residues as in (a) and (b), respectively. (e) Surface representations for the hydrophobic pocket of the GRAMD1A-S homology model (top) and the crystal structure of GRAMD1C-S (bottom) with docked 25(OH)-cholesterol (magenta) and autogramin-2 (cyan), viewed from two different angles, colored by the electrostatic potential. (f) Ligand contact plots showing the interaction of GRAMD1A-S with docked 25(OH)-cholesterol and autogramin-2.

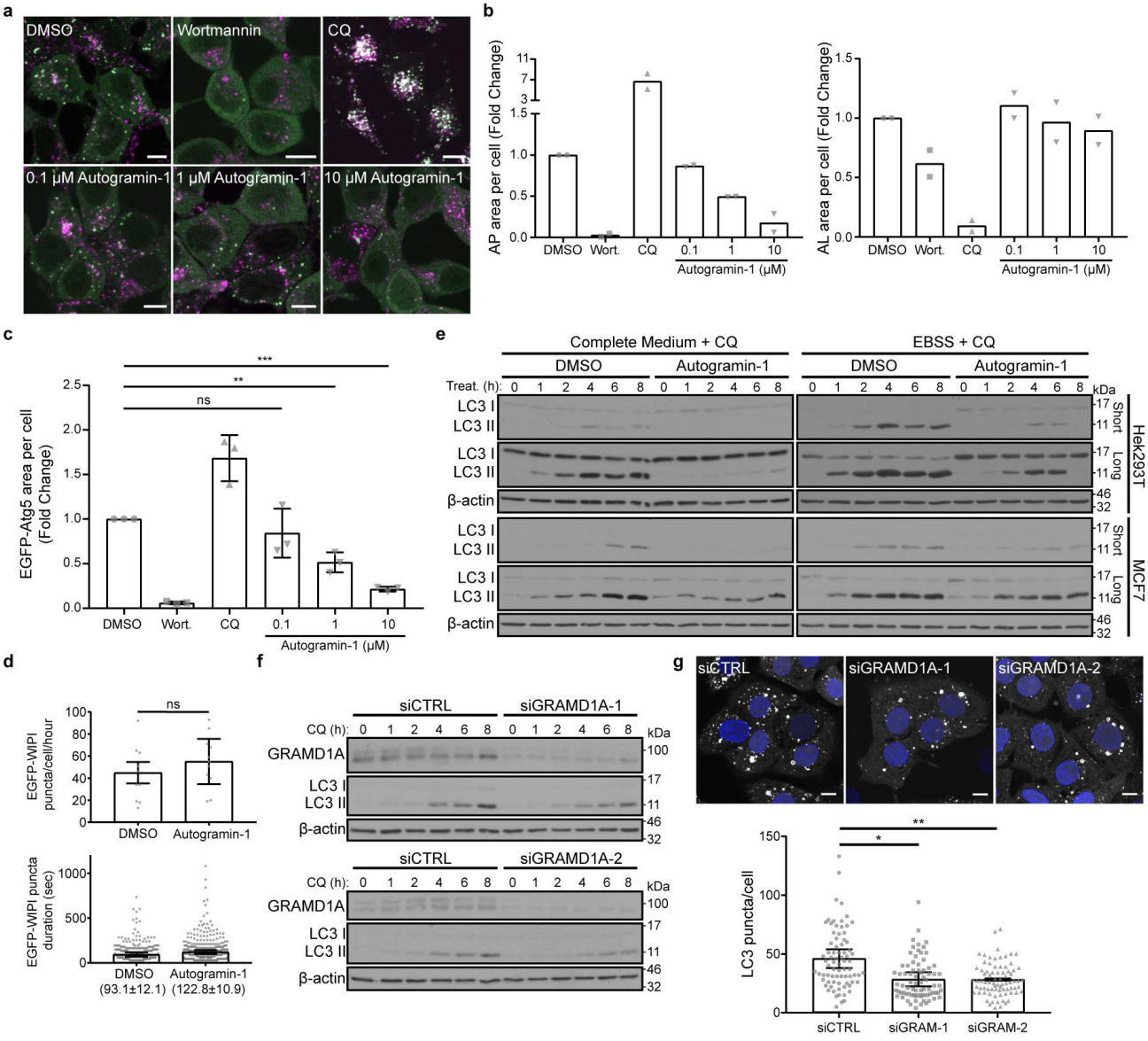

Figure 5. GRAMD1A is required for autophagy initiation. (a) MCF7 mCherry-EGFP-LC3 cells serum starved and treated with 500 nM wortmannin, 50 μM chloroquine (CQ) or autogramin-1 for 3 h. Scale bar, 10 μm. Magenta: mCherry. Green: EGFP. (b) Autophagosomes (AP) and autolysosomes (AL) from (a) were quantified and data represented as the fold change in AP/AL area per cell, relative to DMSO control. Data points represent 3 biologically independent experiments, bar graphs show mean ± SD. P-values were derived from biological replicates using a two-tailed, unpaired t-test. ns =not significant, ** p=0.0003. *** p<0.0001. (c) MCF7 EGFP-ATG5 cells were starved and treated with 500 nM wortmannin, 50μM CQ or autogramin-1 for 3 h. Phagophores (green puncta) were quantified and data represented as the fold change in EGFP-Atg5 area per cell, relative to DMSO treated cells. Data points represent 3 biologically independent experiments, bar graphs show mean ± SD. P-values were derived from biological replicates using a two-tailed, unpaired t-test. ns =not significant, ** p=0.0017. *** p<0.0001. (d) Hek293 cells stably expressing EGFP-WIPI2b were treated with EBSS and DMSO or 5 μM Autogramin-1 and imaged every 15 sec for 1 hour. Total number (top) and average duration (bottom) of EGFP-WIPI2b puncta were quantified. Bars show mean ± SD from 3 biologically independent experiments. Data points represent individual cells (top) and puncta (bottom) pooled from the 3 independent experiments. P-values were derived from biological replicates using a two-tailed, unpaired t-test. ns = not significant. (e) Western blot analysis of MCF7 and HEK293T cells treated with DMSO or autogramin-1 in the presence of 50 μM CQ for indicated time points. Data are representative of two independent experiments. Uncropped blots found in Supplementary Figure 10. (f) Western blot analysis of MCF7 cells transfected with a control or one of two GRAMD1A targeting siRNAs for 24 h. Data are representative of two independent experiments. Uncropped blots found in Supplementary Figure 10. (g) MCF7 EGFP-LC3 cells were transfected with a control or GRAMD1A targeting siRNA for 24 h. (Top) Cells were treated with 50 μM CQ for 3 h and imaged by confocal microscopy. Scale bar, 10 μm. (Bottom) Quantification of LC3 puncta per cell. Bars show mean ± SD from 3 biologically independent experiments. Data points represent individual cells pooled from the 3 independent experiments. P-values were derived from biological replicates using a two-tailed, unpaired t-test. * p=0.0377. ** p=0.0180.

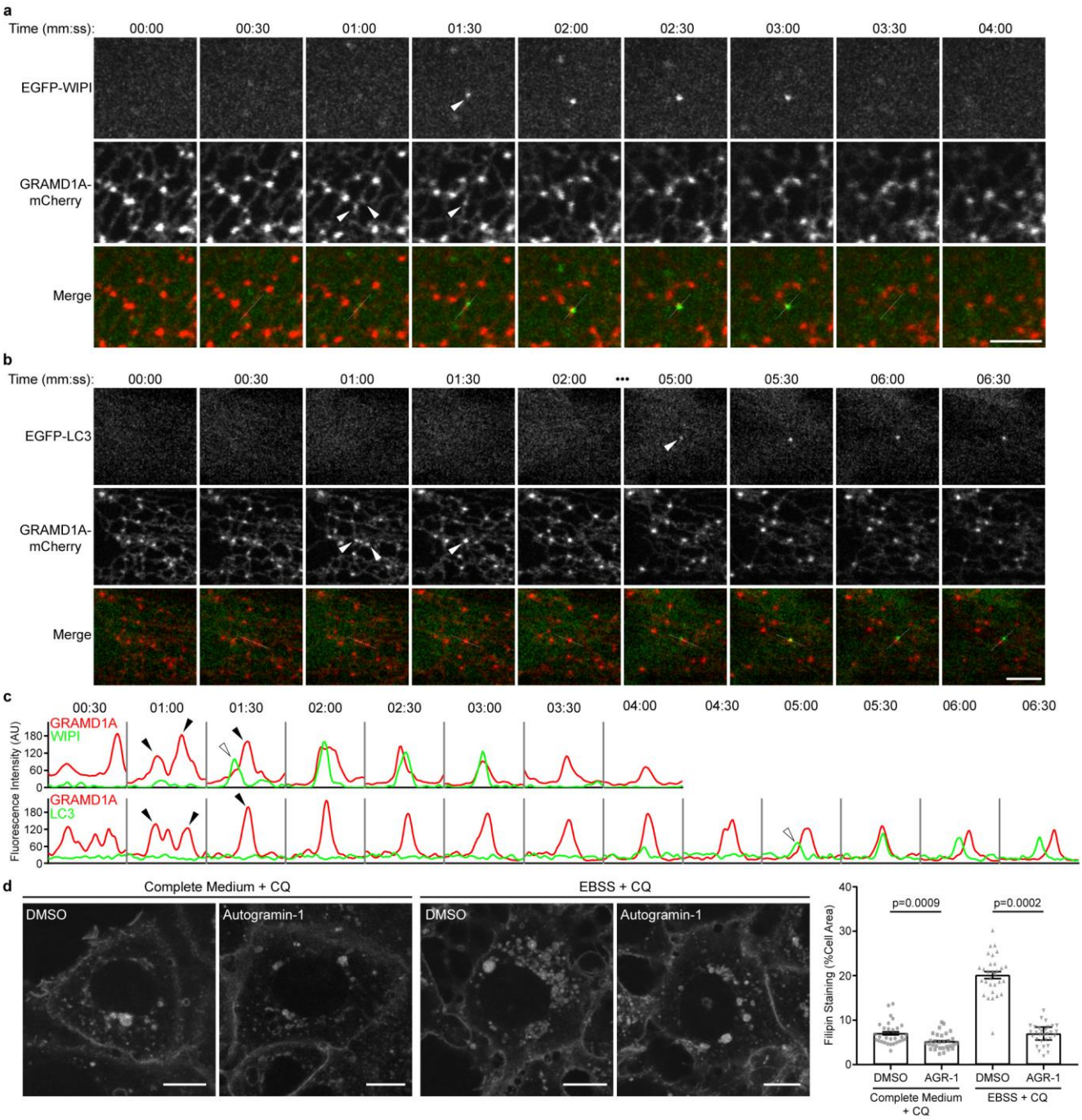

Figure 6. GRAMD1A is localized to sites of autophagosome initiation. (a) HeLa cells co-transfected with EGFP-WIPI1 and GRAMD1A-mCherry undergoing starvation. Frames captured every 30 seconds. White arrowheads indicate the site of WIPI1 emergence/GRAMD1A enrichment. Scale bar, 4 µm. Data are representative of two independent experiments. (b) HeLa cells co-transfected with EGFP-LC3 and GRAMD1A-mCherry undergoing starvation. Frames captured every 30 seconds. White arrowheads indicate the site of LC3-positive autophagosome formation/GRAMD1A enrichment. Scale bar, 4 µm. Data are representative of five independent experiments. (c) Profiles of fluorescence intensity along dotted white lines in the corresponding merged images in (a) and (b). (d) MCF7 cells treated as indicated

and stained with filipin to visualize free cholesterol (left). Scale bars, 10 μm. Quantification of filipin staining (right). Bars show mean ± SD from 3 biologically independent experiments. Data points represent individual cells pooled from the 3 independent experiments. P-values were derived from biological replicates using a two-tailed, unpaired t-test. ** p=0.0009. *** p=0.0002.

Online Methods

Chemical synthesis

Syntheses were carried out as described in the supplementary note “Synthetic Procedures”.

Cell Culture and Transfection

HEK293T (ATCC) and HeLa (ATCC) cells were cultured in Dulbecco’s modified Eagle’s medium (Sigma) supplemented with 10% fetal calf serum, 1% penicillin/streptomycin, and non-essential amino acids at 37°C with 5% CO_2. MCF7 cells stably transfected with EGFP-LC3 (MCF7-eGFP-LC3) were cultured at 37 °C with 5% CO_2 using Eagle’s MEM (PAN Biotech cat# P04-08500) containing 10% FBS (Invitrogen cat# 10500-084), 1% sodium pyruvate (PAN Biotech cat# P04-43100), 1% NEAA (PAN Biotech cat# P08-32100), 0.01 mg/ml bovine insulin (Sigma Aldrich cat# I9278) and 200 µg/ml G418 as the medium. Untransfected MCF7 cells were incubated in the same media without G418. Cells were tested for mycoplasma contamination bimonthly using the MycoAlertTM mycoplasma detection kit (Lonza). Transfection of DNA constructs and siRNAs were performed using X-tremeGENE HP transfection reagent (Roche) and Lipofectamine 3000 (Invitrogen), respectively, according to the manufacturer’s directions.

High-content screening for autophagy inhibitors

The phenotypic autophagy screen utilizes MCF7-eGFP-LC3 cells. 4000 cells per well were seeded in 25 µl medium in a 384 well Greiner µclear plate (cat# 781080, lid cat# 656191) and incubated (37 °C, 5% CO2) overnight. Cells were then washed by a plate washer (Biotek, ELx405) three times with 1X PBS followed by a final aspiration of the washing buffer. The addition of 25 nl of compound solution (10 mM stock solution in DMSO) was then carried out with an echo dispenser (Labcyte, Echo 520 dispenser). Addition of medium to induce autophagy was carried out with a Multidrop Combi (Thermo Scientific). 25 µl EBSS (Sigma Aldrich, cat# E3024-500ml) containing 50 µM Chloroquine (Sigma Aldrich, cat# C6628-25g) was used for starvation-induced autophagy and 25 µl medium containing 50 µM Chloroquine and 100 nM Rapamycin (Biomol, cat# Cay13346)-1 was used for rapamycin-induced autophagy screening. After incubation (37 °C, 5% CO_2) for three hours cells were fixed by addition of 25 µl 1:4 formaldehyde in 1X PBS + 1:500 Hoechst (stock: 1 mg/ml, Sigma Aldrich cat# B2261-25mg) and incubation for 20 min at room temperature. Cells were then washed three times with 1X PBS. Four images per well were taken with ImageXpress Micro XL (Molecular Devices) at 20x. Automated image analysis was performed using the granularity setting of MetaXpress Software (Molecular Devices). The most significant analysis parameter was granule area; with resulting signal-to-background ratios around 40 and Z’ values around 0.7.

Antibodies

Anti-p62/SQSTM1 was purchased from MBL international (Cat# PM045) and used at 1:10000. Anti-LC3B was obtained from Cell Signaling Technology (Cat# 2775) and used at 1:1000. Anti-beta-actin was purchased from abcam (Cat# ab8227) and used at 1:10,000. Anti-GRAMD1A was purchased from Novus (Cat# NBP1-93730) and used at 1:1000. Anti-GRAMD1B was purchased from Thermo Fischer (Cat# PA5-31387) and used at 1:1000. Anti-GRAMD1C was purchased from Novus (Cat# NBP1-90559) and used at 1:1000. Goat anti-rabbit-HRP was purchased from Pierce (Thermo Scientific, Cat# 31460) and used at a dilution of 1:10,000. Anti-His-tag monoclonal antibody was obtained from Cell Signaling Technology (Cat# 2366) and used at 1:1000. Goat anti-mouse HRP secondary antibody was purchased from Thermo Fisher (Cat# 31430) and used at 1:10,000.

Immunoblotting

For the initial validation of autogramins, 200,000 MCF7-eGFP-LC3 cells in 2 mL media were seeded in 6-well plates and incubated (37 °C, 5% CO_2) overnight. The media was removed and the cells were washed with PBS (1X), before adding test compounds at the required concentrations in EBSS. Cells were incubated (37 °C, 5% CO_2) for 3 h before removing the media, washing with PBS (1X), and lysing in SDS loading buffer without bromophenol blue. Protein concentrations were determined using the DC Assay (Bio-rad) according to the manufacturer's instructions. SDS-PAGE was carried out using 15% polyacrylamide gels run at a constant voltage of 80 V for 15 min followed by 120 V for approximately 2 h. Semi-dry transfer onto a PVDF membrane was performed at 25 V for 45 min. Membranes were blocked in 5% milk in TBST (blocking buffer) for 1 h at room temperature. The membrane was incubated with the primary antibody in blocking buffer overnight at 4 °C. After washing with TBST (3 x 5 min) the membrane was incubated with the secondary antibody in blocking buffer for one hour at room temperature. Signals were visualized using the SuperSignal West Pico Chemiluminescent Substrate or the SuperSignal West Femto Maximum Sensitivity Substrate (Thermo Fischer) on a Li-COR Odyssey Fc.

Alternatively, cells were lysed in ice-cold lysis buffer (20 mM Tris-HCl pH 8, 300 mM KCl, 10% Glycerol, 0.25% Nonidet P-40, 0.5 mM EDTA, 0.5 mM EGTA, 1 mM PMSF, 1x complete protease inhibitor (Roche)), passed 5x through a 21G needle, and cleared by centrifugation. Protein concentrations were determined using Bio-Rad Protein Reagent (Bio-Rad). Lysates were then mixed with 2x sample buffer and boiled for 10 min prior to separation by SDS-PAGE and transferred to a nitrocellulose membrane (GE). Membranes were incubated with primary antibody overnight at 4°C, washed with TBST and incubated for 1 h at room temperature with the appropriate HRP-conjugated secondary antibody in

blocking buffer (5% skim milk in TBST). Protein detection was carried out using chemiluminescence (Thermo Scientific) and radiographic film (Santa-Cruz).

WST-1 viability assay

4000 MCF7-GFP-LC3 cells in 100 µL medium were seeded in a clear flat-bottomed 96-well plate and incubated overnight. The media was removed gently, and cells were washed with 1X PBS (100 µL). The PBS was replaced with 100 µL of DMEM with 25 mM glucose (fed conditions) or DMEM with 0 mM glucose (starved). To this were added test compounds at a concentration of 6x the desired final concentration in 20 µL of the appropriate medium. Cells were incubated at 37 °C for 48 h. At this point 10 µL of WST-1 reagent (Roche) was added to each well. The absorbance was measured with a Beckman DTX-880 (Beckman Coulter, Germany) plate reader at 450/690 nm. Absorbance measurements were performed after 20, 30, 40, 50, 60 min of addition. Good measurements are considered when absorbance of the negative control is around 1.00. Growth inhibition (GI_{50}) values were calculated using GraphPad Prism using DMSO (negative) and no cells (positive) as controls.

Incucyte Zoom Live-cell imaging

4000 MCF7 cells in 100 µL medium were seeded in a clear flat-bottomed 96-well plate and incubated overnight. The media was removed gently, and cells were washed with 1X PBS (100 µL). The PBS was replaced with 100 µL of DMEM or DMEM without glucose. To this were added test compounds at a concentration of 6x the desired final concentration in 20 µL DMEM. Cells were incubated at 37 °C in the Incucyte Zoom (Essen BioScience). Images were acquired at 10X magnification in the phase channel every hour. Images were analyzed using automated image analysis. Key parameters were confluence (%). Data was expressed as a percentage of the DMSO treated sample.

NanoBRET target engagement

The gene encoding GRAMD1A-StART domain (*GRAMD1A*$^{359-547}$) was PCR amplified from a human cDNA library and subcloned into a pFN31K or pFC32K vector (Promega) to generate N- or C-terminal NanoLuc fusions, respectively. HeLa cells (DSMZ, Cat.# ACC57) were transferred to OptiMEM (Gibco) supplemented with 4% Fetal Bovine Serum (Gibco). 0.2 µg DNA (pFN31K-GRAMD1A-StART for N-terminal NanoLuc^{R} fusion protein or pFC32K-GRAMD1A-StART for C-terminal NanoLuc^{R} fusion protein), 2 µg Transfection Carrier DNA (Promega) and 15 µL FuGENE HD (Promega) were incubated for 20 min at room temperature. The transfection mix was added to $2x10^6$ cells and incubated for 24 h at 37°C and 5% CO_2. Transfected HeLa cells were resuspended in OptiMEM supplemented with 4% Fetal Bovine Serum, $1x10^4$ cells were seeded into white Bio CELLSTAR 96-well plate (Greiner) and incubated with 0.5 µM Bodipy-Autogramin diluted in Tracer Dilution Buffer (Promega) for 20 min. Cells

were treated with increasing concentrations of Autogramin-2 for 3 h before adding 20 µL 6x NanoBRET™ Nano-Glo® substrate plus 60 µM Extracellular NanoLuc® Inhibitor (Promega) in OptiMEM with a total assay volume of 120 µL. BRET measurements were performed with a Tecan Spark microplate reader equipped with a Luminescence Multi Color System (donor 445 nm-485 nm, acceptor 610 nm-700 nm). Raw BRET ratios (acceptor emission value divided by donor emission value) were then converted in milliBRET units (mBU), corrected for background and normalized to the respective DMSO control. Resulting BRET ratios were plotted against the concentration of autogramin-2 and fitted with GraphPad Prism 6 to the following equation: Y=bottom + (top-bottom)/(1+10^((logEC_{50}-X)*HillSlope)) with Y as normalized BRET ratio and X as decadic logarithm of the autogramin-2 concentration.

Cellular thermal shift assay (CETSA)

For CETSA experiments, MCF7-eGFP-LC3 cells were employed. For one T175 flask (90% confluent), the cells were detached with 3 mL trypsin/EDTA, resuspended in MEM medium (10 mL), and centrifuged at 150 x g and 4 °C for 5 min. The medium was removed and the cell pellet washed with ice-cold 1X PBS (2 x 25 mL and 1 x 10 mL, centrifugation at 150 *x g* and 4 °C for 5 min each time). The pellet was resuspended in PBS containing NP-40 alternative (1.5 mL, 0.4% v/v), in order to enhance membrane protein solubilization. The cells were lysed via a freeze-thaw cycles with liquid nitrogen (4 times). The insoluble components were separated by centrifugation for 20 min at 4 °C and 100,000 g using polycarbonate tubes (Beckmann Coulter) in an ultra-centrifuge. Protein concentration was determined using a Bradford assay. After diluting the lysate to 2 mg/mL, aliquots were snap-frozen and stored at -80 °C until further use.

The cell lysate was thawed and split into two vials (1.4 mL each). One sample was treated with the respective compound of interest and the other with DMSO, resulting in a final concentration of 2.5 µM and 1% (v/v) DMSO. The samples were incubated at room temperature for 30 min, each split into 10 aliquots of 120 µL and subjected to heating at different temperatures in a PCR cycler (Eppendorf, Mastercycler, ep*gradient* S) for 3 min. The temperature gradient ranged from 37–67 °C, while one vehicle sample was always heated in parallel with its respective compound sample. The samples were then cooled to 4 °C, centrifuged for 20 min at 4 °C and 100,000 g. The supernatant (100 µL) was transferred into low-binding Eppendorf tubes. The samples were then diluted with SDS loading buffer and analysed by Western blot.

Differential scanning fluorimetry (DSF)

GRAMD1A-C StART domains were incubated at a concentration of 0.5 mg/mL in absence or presence of 25-hydroxycholesterol or autogramin-2, respectively, for 30 min at room temperature in 20 mM Hepes, pH 7.5, 300 mM NaCl and 2 mM DTE. Subsequently, SYPRO orange (Thermo Fisher) was added at 5x concentration and fluorescence intensity was measured in a CFX96 Real-Time System with C1000 Touch Thermal Cycler (Bio-Rad) with an initial incubation at 25 °C for 5 min followed by steps of 0.2 °C up to 95 °C with 5 sec incubation each. Melting temperatures were calculated with GraphPad Prism 6.

Fluorescence polarization (FP)

Fluorescence polarization experiments were performed at room temperature in 20 mM Hepes, pH 7.5, 300 mM NaCl, 0.01% (v/v) Tween-20 and 2 mM DTE in a final volume of 100 µL in black, flat-bottom, non-binding 96-well plates (Greiner). For K_d determination, 20 nM (6- or 22-) *N*-(7-Nitrobenz-2-Oxa-1,3-Diazol-4-yl)Amino-cholesterol (NBD-cholesterol) or 20 nM Bodipy-autogramin, respectively, was incubated with increasing concentrations of protein of interest for 30 min. For competition experiments, 20 nM 22-NBD-cholesterol or Bodipy-autogramin, respectively, were mixed with 150 nM of proteins of interest or 600 nM of GRAMD1B-GS and incubated with increasing concentrations of 25-hydroxycholesterol or autogramin-2, respectively, for 30 min. For the NBD-cholesterol experiments, the fluorescence polarization signal was measured using a Safire 2 multimode microplate reader (Tecan) with an excitation at 470 nm and an emission at 535 $\pm$ 5 nm. In case of Bodipy-autogramin, signals were measured using a Spark multimode microplate reader (Tecan) with a filter-based excitation at 540 nm and a filter-based emission at 590 nm. Data were visualized and fitted with GraphPad Prism 6 to the following equation: Y=bottom + (top-bottom)/(1+10^((logEC_{50}-X)*HillSlope)) with Y as FP signal and X as decadic logarithm of the protein or ligand concentration. K_i values were calculated using the following equation: $K_i=IC_{50}/(1+[L]/K_d)$ with [L] as concentration of labeled ligand and K_d as dissociation constant for the labeled ligand.

Vesicle preparation

Stock solutions were prepared of 1,2-dioleoyl-*sn*-glycero-3-phosphocholine (DOPC, Avanti Polar Lipids) in chloroform (10 mg/mL) as well as of the fluorescently labeled lipids 23-(dipyrromethaneboron difluoride)-24-norcholesterol (TopFluor® Cholesterol, Avanti Polar Lipids) (TF-Chol) and *N*-(lissamine™ rhodamine B sulfonyl)-1,2-dihexadecanoyl-*sn*-glycero-3-phosphoethanolamine (ammonium salt) (*N*-Rh-DHPE, Life Technologies) in methanol (100 µM) and mixed to obtain the lipid mixture DOPC/TF-Chol/*N*-Rh-DHPE with a molar ratio of 99:0.5:0.5. The appropriate amount of DOPC and the lipid mixture was used to prepare large unilamellar vesicles (LUVs). After most of the solvent was evaporated with a nitrogen steam, remaining chloroform/methanol was removed under vacuum for at least 2 h. The dried

lipid films were hydrated with a buffer containing 20 mM Hepes, pH 7.5, 300 mM NaCl, and 2 mM DTE. After extensive vortexing and sonication for 5 min in a water bath at 40 °C, large multilamellar vesicles were generated by five freeze-thaw cycles and a subsequent sonication for 5 min. This multilamellar vesicles could be transformed to LUVs of homogenous size by extrusion 21 times through a polycarbonate membrane (Avanti Polar Lipids, Alabaster USA) with a pore size of 100 nm at 40 °C.

Cholesterol transfer assay

The transfer of cholesterol between donor and acceptor vesicles was monitored by a FRET-based assay with TF-Chol and *N*-Rh-DHPE as FRET pair. Donor vesicles were prepared from the lipid mixture DOPC/TF-Chol/*N*-Rh-DHPE (99:0.5:0.5, molar ratio) exhibiting a high FRET signal at 590 nm upon excitation at 488 nm due to the proximity of both fluorescent lipid analogues. The protein-catalyzed extraction and transfer of TF-Chol to acceptor vesicles consisting of pure DOPC resulted in a decreased FRET signal.

The time-resolved measurements were performed using a Hi-Tech Scientific SF-61SX2 stopped-flow spectrometer (TgK Scientific, Bradford on Avon, U.K.). A Xe arc lamp was used to excite the samples at 488 nm and fluorescence emission was recorded through a 590 nm cutoff filter. For all experiments, the reactant syringes were filled with 40 µM donor vesicles and 40 µM acceptor vesicles in presence of 0.34 µM protein, respectively. Both solutions were rapidly mixed in the mixing chamber, where concentration of each component is only half. For experiments in presence of the inhibitor, the proteins were pre-equilibrated with various amount of the inhibitor (0-20 µM) for 30 min at room temperature before mixing with donor vesicles in presence of acceptor vesicles in the stopped-flow apparatus. 5-10 single injections were accumulated for each experiment. At least 3 independent experiments were performed for each condition. All measurements were carried out at 25 °C in buffer containing 20 mM Hepes, pH 7.5, 300 mM NaCl and 2 mM DTE. Time traces could be best fitted to the following bi-exponential equation indicating a biphasic binding process:

$$F(t) = F_0 + A_1\left(1 - e^{-k_{obs,1}t}\right) + A_2\left(1 - e^{-k_{obs,2}t}\right)$$

Here, F(t) is the fluorescence signal corresponding to the concentration of the extracted cholesterol at time t. The amplitudes A_1 and A_2 are for the first and second binding phase, respectively. $k_{obs,1}$ and $k_{obs,2}$ represent the observed rate constants for the first and second binding step, respectively, and F_0 is the fluorescence offset representing the final fluorescence intensity.

Atomic force microscopy (AFM)

Large unilamellar vesicles containing DOPC/DPPC/Cholesterol at a molar ratio of 1:2:1 were prepared as described above. Vesicle fusion on mica was carried out by depositing 70 µL of the large unilamellar vesicles (LUV) solution on freshly cleaved mica and incubation in a wet chamber at 70 °C for 2 h. The

samples were rinsed carefully with Tris buffer to remove unspread vesicles. For the protein-membrane interaction studies 200 µL of 1 µM GRAMD1A StART domain were injected into the AFM fluid cell at room temperature. Measurements were performed on a MultiMode scanning probe microscope with a Nano-Scope IIIa controller (Digital Instruments, Santa Barbara, CA) and a J-Scanner (scan size 125 µm). Images were obtained by applying the tapping mode in liquid with oxide-sharpened silicon nitride (DNP-S) or sharp nitride lever (SNL) probes mounted in a fluid cell (MTFML, Veeco (now Bruker), Karlsruhe, Germany). Tips with nominal force constants of 0.24 N/m were used at driving frequencies around 9 kHz and drive amplitudes between 200 and 800 mV. Scan frequencies were between 1.0 and 1.94 Hz. Height images of sample regions were acquired with resolutions of 512 × 512 pixels. All measurements were carried out at room temperature and analyzed by using the analysis and processing software NanoScope version 5.

PIP strips

PIP strips (Echelon Biosciences) were blocked with 10 mL blocking buffer (20 mM Hepes, pH 7.5, 300 mM NaCl, 0.1% (v/v) Tween-20 and 3% (w/v) fatty acid free BSA) for 1 h. Subsequently, the membranes were incubated with 10 mL blocking buffer containing 10 µg/mL of His_6-tagged protein of interest for 1h. After washing three times with 10 mL of washing buffer (20 mM Hepes, pH 7.5, 300 mM NaCl and 0.1% (v/v) Tween-20) for 5-10 min each, anti-His-tag monoclonal antibody (Cell Signaling) was added to the PIP strips diluted 1:1,000 in 10 mL blocking buffer for 1 h. The membranes were washed again as described above and incubated with goat anti-mouse HRP secondary antibody (Thermo Fisher) diluted 1:10,000 in blocking buffer. After another washing, HRP signal was detected using the SuperSignal West Pico Chemiluminescent Substrate or the SuperSignal West Femto Maximum Sensitivity Substrate (Thermo Fischer) on a Li-COR Odyssey Fc. All incubation and washing steps were performed at room temperature under gentle agitation.

Hydrogen deuterium exchange mass spectrometry (HDX-MS)

GRAMD1A-S was dialyzed over night in 2 L equilibration buffer (10 mM Hepes, pH 7.5, 300 mM NaCl and 1 mM TCEP) at 4 °C. Dialyzed GRAMD1A-S at a concentration of 0.1 mg/mL was incubated with 5x molar excess of 25-hydroxycholesterol or autogramin-2, or equivalent amounts of respective solvent (ethanol in case of 25-hydroxycholesterol and DMSO in case of autogramin-2) for 1 h on ice. Using an automated pipetting platform (HDx-2 PAL, LEAP), 3 µL GRAMD1A-S in absence or presence of 25-hydroxycholesterol or autogramin-2, respectively, were incubated with 55 µL equilibration or deuteration buffer at 20 °C for different exposure times. The deuteration buffer was prepared with the identical composition as the equilibrium buffer, but with D_2O instead of H_2O. The pD was adjusted with DCl/NaOD to pH^{app} of 7.1 ($pD = pH^{app} + 0.4$). 50 µL of the reactions were mixed with 50 µL quenching buffer (100

mM KPi pH 2.6, 10 mM TCEP and 6 M urea) at 0 °C. Subsequently, 50 µL were digested on a pepsin column (Enzymate BEH Pepsin Column 2.1mm*30mm, Waters) at 20 °C and resulting peptides were trapped at 0°C onto a pre-column (Acquity UPLC BEH C18 1.7µm VanGuard 2.1*5mm, Waters) using 0.1% formic acid in water as eluent with a flow rate of 200 µL/min for 3 min, with eluent flow to waste to remove the previously used buffers. The separation of the peptides was performed at 0 °C on a nanoAcquity UPLC (Waters) by back-flushing the sample during the whole analysis from the pre-column to the analytical column (Acquity UPLC BEH C18 1.7µm 1.0*100mm, Waters) using a linear gradient starting with 95% solvent A (water containing 0.1% formic acid) / 5% solvent B (acetonitrile containing 0.1% formic acid) and increasing to 65% solvent A / 35% solvent B within 7 min using a flow rate of 40 µL/min. After two washing steps the column was re-equilibrated to starting conditions. For mass recalibration a lock mass (Leucine, Waters, 200 pmol/µl at 10 µl\min) was recorded every 45 s. The LC was online coupled to the MS via ESI-source with a capillary voltage of 3.0 kV. Mass spectra were measured with a mass range of 50 Da to 2000 Da in resolution mode with activated ion mobility separation. MS^E was measured with a low CE of 10.0 V and a high CE of 30.0 V. Six replicates were measured for the undeuterated samples and four replicates for each deuterated sample.

Data of the undeuterated samples were processed with ProteinLynx Global SERVER (PLGS) 3.0.3 software (Waters) to identify peptides. Afterwards, data of deuterated and undeuterated samples were analyzed with DynamX 3.0 software (Waters) to quantify the deuteration uptake using the peptides identified by PLGS. The automated peak identification by DynamX was manually corrected. Here, also the drift time information obtained from the ion mobility mode was used for accurate peak identification. “False EX1” peaks[43], which most prominently appeared at long exposure times and therefore probably arose from protein aggregation, were excluded. Visualization of the relative deuterium uptake of ligand-bound vs. ligand-unbound state was done with DynamX and resulting difference heat maps were exported as pymol scripts. Pymol scripts for the different exposure times were combined to a single file that contained the highest deuterium uptake differences of ligand-bound vs. ligand-unbound state for each residue.

Crystal structure determination

The StART domain of GRAMD1C (residues 318-504 plus the N-terminal PreScission site cloning artifact “GPLGS”, native and SeMet-labeled) purified from *E. coli* strain C41 was used for crystallization at a concentration of 10 mg/ml. Crystals were obtained at 20 °C in hanging drops containing 0.1 M Hepes, pH 7.0, 40% (v/v) MPD and 10% (w/v) PEG8000. Crystals were mounted in a thin film of mother liquor without additional cryo protectant. A selenomethionine SAD (single anomalous diffraction) data set was collected at a wavelength of 0.97793 Å and a temperature of 100 K using a Pilatus 6M detector at the

X10SA beamline at the SLS in Villigen, Switzerland, integrated and scaled using XDS and XSCALE[44] and solved with selenium-SAD phasing using CRANK2 from the CCP4 package. All three selenium sites were found (FOM: 0.329, 0.605 after density modification) and the quality of the initial phases was sufficient for automatic building of most of the single GRAMD1C chain in the asymmetric unit of the monoclinic unit cell. Model refinement was performed with Phenix[45] and Coot[46]. The Ramachandran plot shows 98.9% of all residues in favored regions, 1.1% in allowed regions and no outliers. The data collection and refinement parameters are shown in Supplementary Table 3. Figures were made using PyMOL (The PyMOL Molecular Graphics System, Schrödinger, LLC).

Homology modeling and docking

The homology modeling of the GRAMD1A StART domain was performed with MODELLER[47] based on the crystal structure of the GRAMD1C StART domain. Docking of 25(OH)-cholesterol and autogramin-2 into the structures of the StART domains of GRAMD1A and GRAMD1C was done with GOLD[48]. Energy minimization was performed with MacroModel of the SCHRÖDINGER Small-Molecule Drug Discovery Suite (Small-Molecule Drug Discovery Suite 2018-1, Schrödinger, LLC, New York, NY, 2018). Figures were made using PyMOL (The PyMOL Molecular Graphics System, Schrödinger, LLC). Ligand contact plots were done with LigPlot+ software[49].

Filipin Staining

Cells were fixed in 3% paraformaldehyde in PBS for 1 h at room temperature and rinsed 3 times with PBS containing 50 mM ammonium chloride. Cells were then stained with a 0.05 mg/mL filipin solution (in PBS + 10% FBS) for 2 h at room temperature. Cells were rinsed 3 times with PBS and imaged immediately.

EGFP-WIPI2b Dynamics

Hek293A EGFP-WIPI2b (kind gift of Sharon Tooze)[12] cells were treated with EBSS to induce autophagy in the presence or absence of autogramin-1. Cells were imaged every 15 seconds for 1 hour and the total number, and average duration of EGFP-WIPI2b foci were quantified using the spot tracking function of the open-source bioimage processing software, Icy[51].

Immunofluorescence

For fixed cell immunofluorescence, cells were fixed in 3% paraformaldehyde in PBS for 10 min at room temperature, washed 3 times with PBS containing 50 mM ammonium chloride, permeabilized in 0.25% Triton X-100 in PBS for 5 min and washed 3 times with PBS. Cells were blocked with 5% donkey serum in PBS and GRAMD1A was visualized using an anti-His antibody (1:400, Cell Signaling #12698)

followed by an Alexa Fluor 647-conjugated anti-rabbit IgG secondary antibody (1:400, Jackson ImmunoResearch # 211-605-109). For live-cell imaging, cells were seeded on 35 mm glass bottom dishes (MatTek, Ashland) and incubated for 24 h. Imaging was performed in MEM without phenol red (Invitrogen) or EBSS (Sigma).

Immunofluorescence imaging was performed on two systems: 1)TCS SP5 AOBS inverted confocal microscope system (Leica Microsystems) equipped with a 63×/1.4 HCX Plan Apo oil immersion lens and a temperature-controlled hood maintained at 37°C and 5% CO_2. 4′,6-diamidino-2-phenylindole (DAPI), EGFP, mCherry and Alexa-647 fluorescence were excited using 405 nm Diode-UV laser, 488 nm WLL, 569 or 594 nm WLL and 633 nm HeNe, respectively. Detection of fluorescence emission was restricted using an Acousto-Optical Beam Splitter approximately as follows: DAPI, 425-450 nm; EGFP, 503-546 nm; mCherry, 600-640 nm, and Alexa-647, 660-700 nm. Scanning was performed in line-by-line sequential mode. 2) Zeiss Cell Observer spinning disk confocal (ANDOR iXon Ultra) (Carl Zeiss) equipped with a 63x immersion oil objective lens (Plan-Apochromat 1.40 Oil DIC M27) and a temperature-controlled hood maintained at 37°C and 5% CO_2. Image processing was restricted to the lowering of background with a Gaussian blur (radius 1 pixel) and brightness/contrast adjustment using ImageJ (NIH). Fluorescence intensity profiles were generated using ImageJ (plot profile command).

Statistical Analysis

Statistical significance (p values) was determined by Student's t tests (two-tailed unpaired) using Prism6 software (GraphPad). *$p \leq 0.05$, **$p \leq 0.01$, ***$p \leq 0.001$, ****$p \leq 0.0001$, NS = non-significant.

Data Availability

The authors declare that the data supporting the findings of this study are available within the paper and its supplementary information files. Additional raw data associated with all figures are available from the corresponding authors upon reasonable request. The atomic structure of the StART domain of GRAMD1C was deposited in the Protein Data Bank under the accession number 6GN5.